Supplementary Information

Concentration-Dependent Supramolecular Self-Assembly of A1/A2-Asymmetric-Difunctionalized Pillar[5]arene

Talal F. Al-Azemi* and Mickey Vinodh

Chemistry Department, Kuwait University, P.O. Box 5969, Safat 13060, Kuwait

Table of contents

* Corresponding author.
E-mail address: t.alazemi@ku.edu.kw.

Single crystal X-ray diffraction data

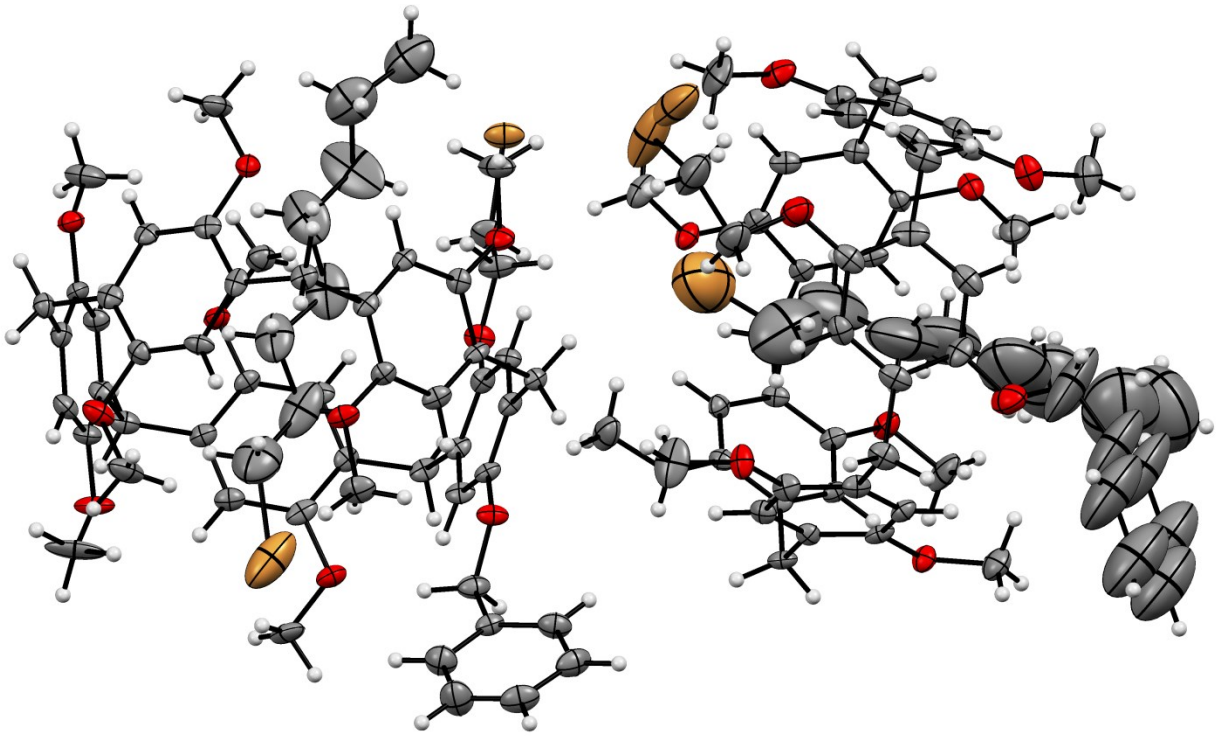

Figure S1. Thermal ellipsoid representation (30% probability) of **Pillar-1a** asymmetric unit. Color code: gray-carbon; red-oxygen, brown-bromine and light gray-hydrogen.

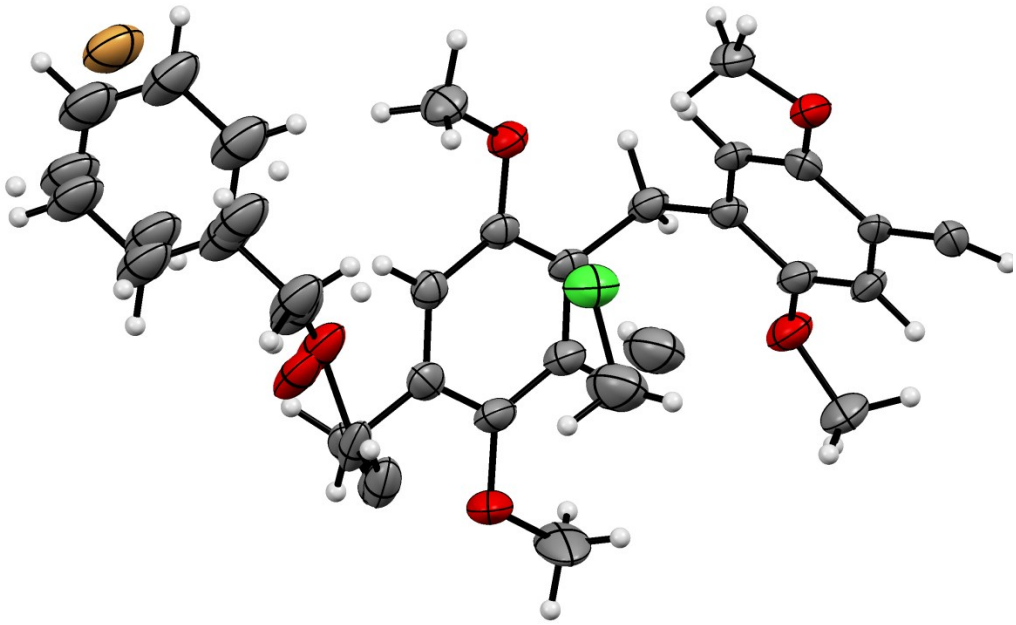

Figure S2. Thermal ellipsoid representation (30% probability) of **Pillar-1b** asymmetric unit. Color code gray-carbon; brown-bromine; red-oxygen; green-chlorine and light gray-hydrogen.

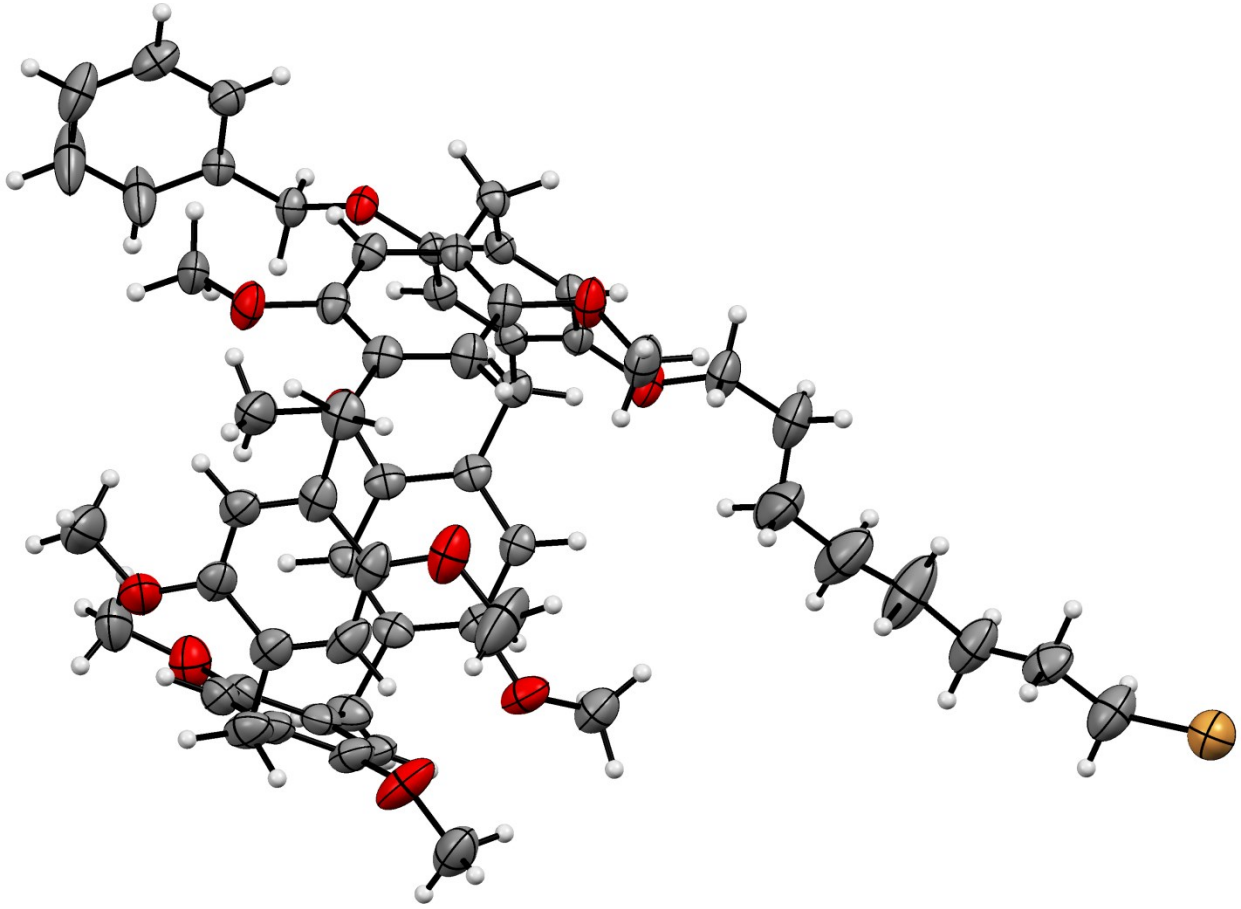

Figure S3. Thermal ellipsoid representation (30% probability) of **Pillar-1a** asymmetric unit. Color code: gray-carbon; red-oxygen, brown-bromine and light gray-hydrogen.

Table S1. Experimental details and crystallographic parameters of **Pillar-1(a-c).**

Sample Name	**Pillar-1c**	**Pillar-1b**	**Pillar-1a**
Chemical formula	$C_{58}H_{67}BrO_{10}$	$C_{56}H_{63}BrCl_2O_{10}$	$C_{60}H_{72}Br_2O_{10}$
M_r	1004.07	1046.87	1112.99
Crystal system, space group	Monoclinic, $P2_1/n$	Monoclinic, $C2/c$	Monoclinic, $P2_1/c$
Temperature (K)	150	150	150
a, b, c (Å)	12.8823 (7), 24.2792 (12), 16.7762 (8)	12.2658 (10), 21.0563 (16), 20.8415 (18)	38.9455 (13), 12.2323 (5), 24.7957 (8)
β (°)	92.983 (7)	103.532 (7)	98.379 (7)
V (Å^3)	5240.0 (5)	5233.3 (8)	11686.4 (7)
Z	4	4	8
Radiation type	Mo $K\alpha$	Mo $K\alpha$	Mo $K\alpha$
μ (mm^{-1})	0.84	0.95	1.44
Crystal size (mm)	0.21 × 0.18 × 0.15	0.20 × 0.14 × 0.11	0.21 × 0.16 × 0.08
Diffractometer	Rigaku R-AXIS RAPID	Rigaku R-AXIS RAPID	Rigaku R-AXIS RAPID
Absorption correction	Multi-scan *ABSCOR* (Rigaku, 1995)	Multi-scan *ABSCOR* (Rigaku, 1995)	Multi-scan *ABSCOR* (Rigaku, 1995)
T_{min}, T_{max}	0.382, 0.881	0.526, 1.000	0.426, 1.000
No. of measured, independent and observed [$I > 2\sigma(I)$] reflections	39119, 9029, 3984	19970, 4600, 2152	75664, 20167, 8409
R_{int}	0.089	0.094	0.162
$(\sin\theta/\lambda)_{max}$ (Å^{-1})	0.594	0.595	0.595
$R[F^2 > 2\sigma(F^2)]$, $wR(F^2)$, S	0.065, 0.183, 1.01	0.099, 0.324, 1.06	0.111, 0.372, 1.06
No. of reflections	9029	4600	20167
No. of parameters	630	373	1311
No. of restraints	3	234	246
H-atom treatment	Constrained	Constrained	Constrained
$\Delta\rho_{max}$, $\Delta\rho_{min}$ (e Å^{-3})	0.37, −0.31	0.68, −0.65	1.48, −1.61

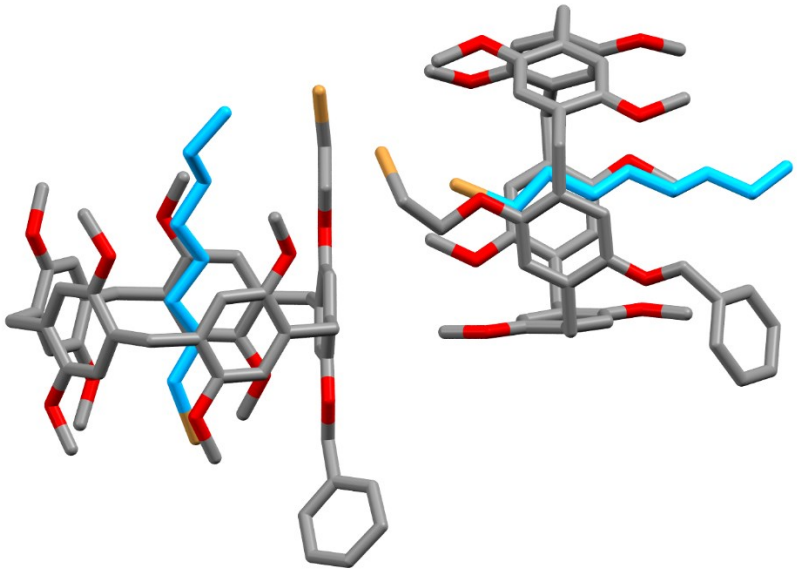

Figure S4. Presentation of the stacking pattern of **Pillar-1a** crystals viewing along crystallographic *b*-axis (hydrogens omitted for clarity).

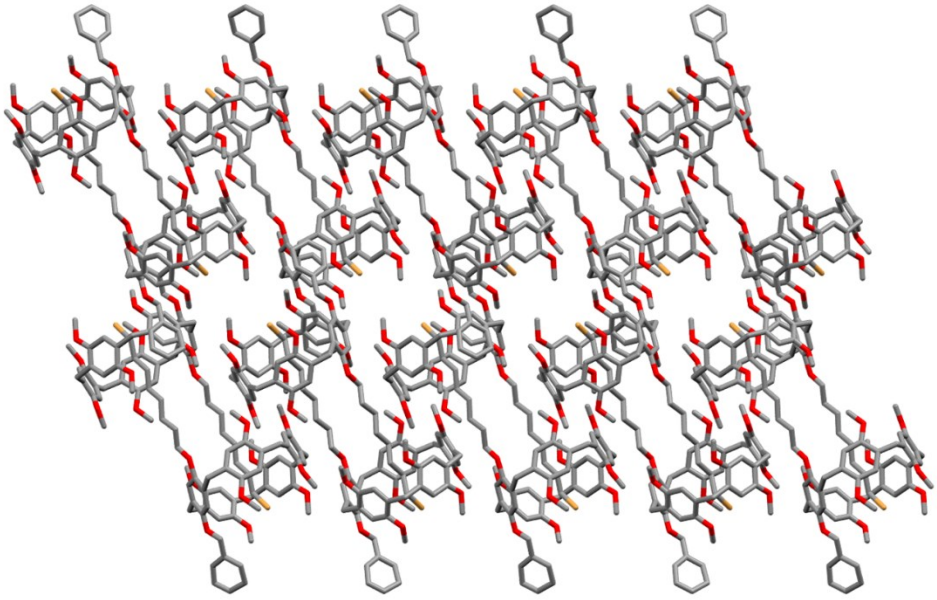

Figure S5. Three-dimensional packing of **Pillar-1c** crystals viewing along crystallographic *b*-axis.

NMR spectra of pillar[5]arene precusors:

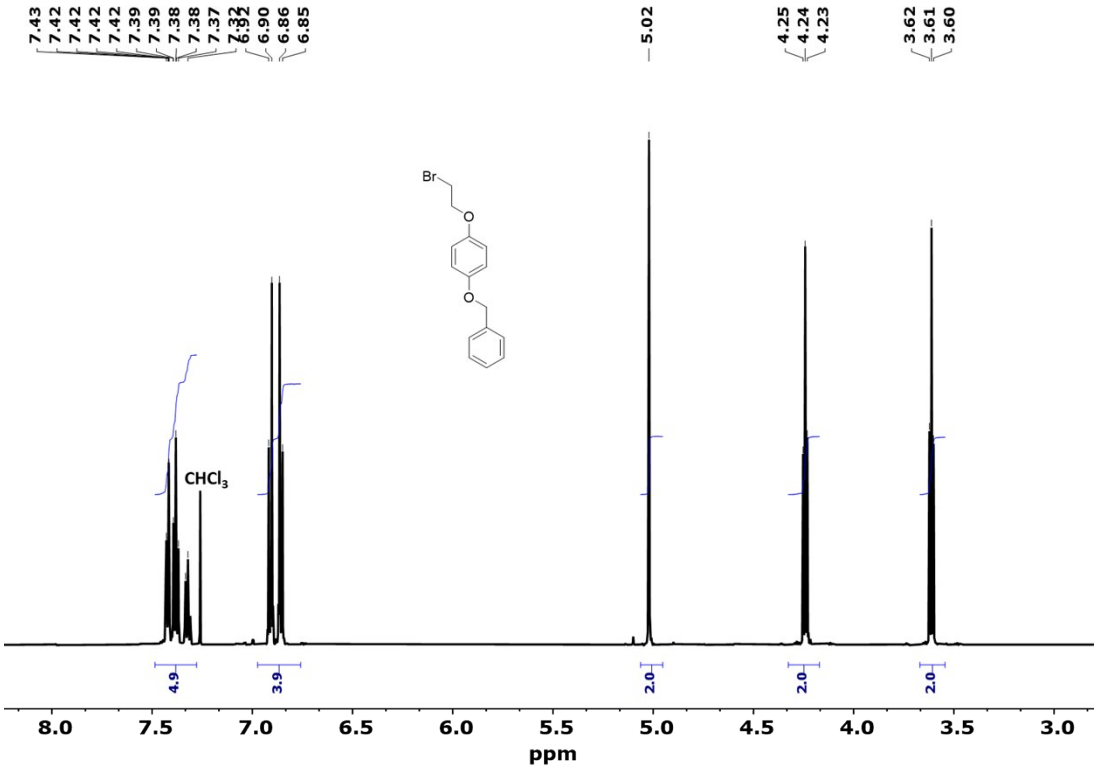

Figure S6. ^{1}HNMR (600 MHz, $CDCl_3$) spectrum of 1-(benzyloxy)-4-(2-bromoethoxy)benzene.

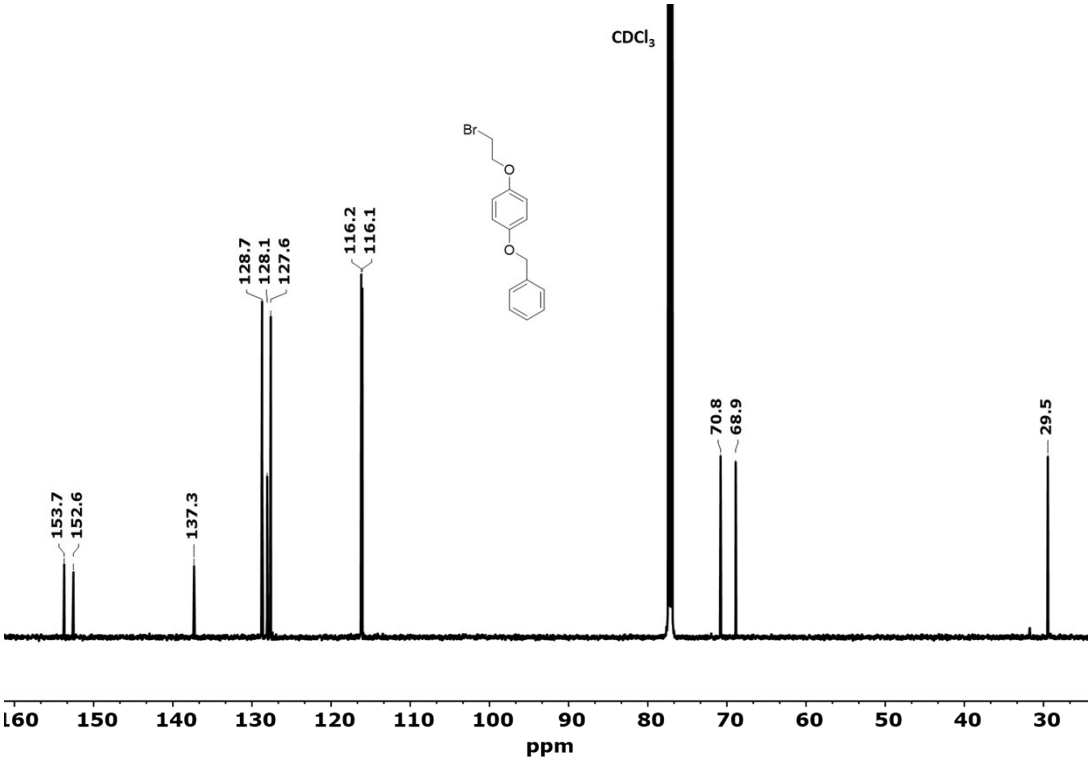

Figure S7. ^{13}CNMR (150 MHz, $CDCl_3$) spectrum of 1-(benzyloxy)-4-(2-bromoethoxy)benzene

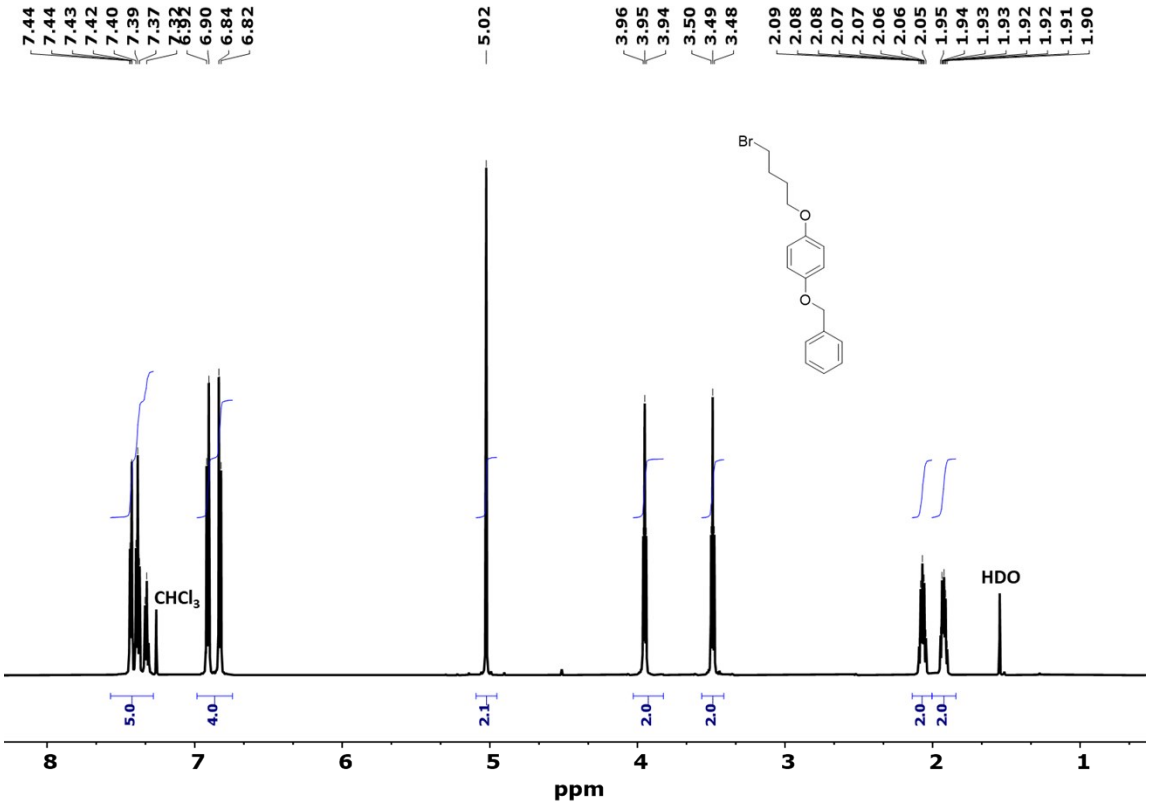

Figure S8. ^{1}HNMR (600 MHz, $CDCl_3$) spectrum of 1-(benzyloxy)-4-(4-bromobutoxy)benzene.

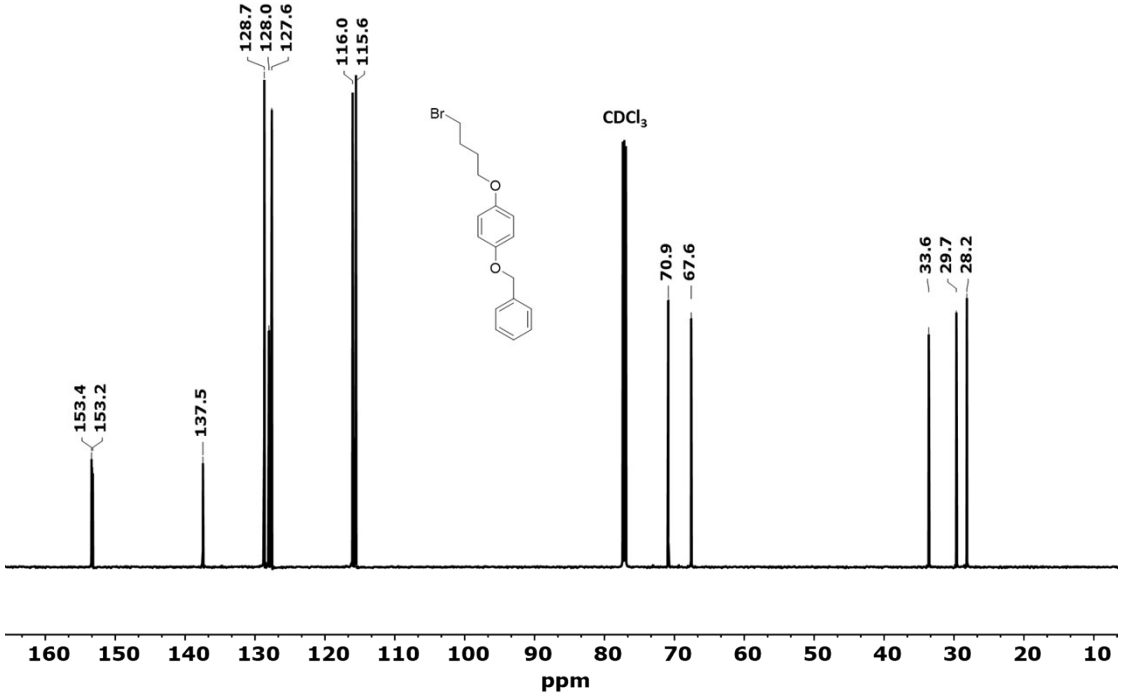

Figure S9. ^{13}CNMR (150 MHz, $CDCl_3$) spectrum of 1-(benzyloxy)-4-(4-bromobutoxy)benzene

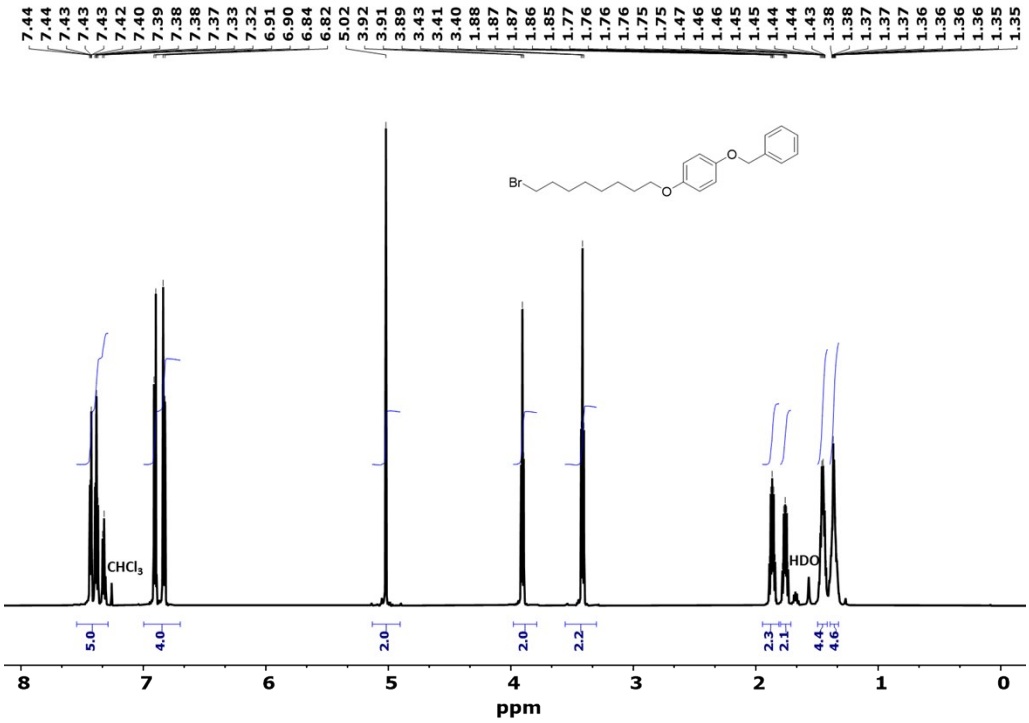

Figure S10. ^{1}HNMR (600 MHz, $CDCl_3$) spectrum of 1-(benzyloxy)-4-(8-bromooctyloxy)benzene.

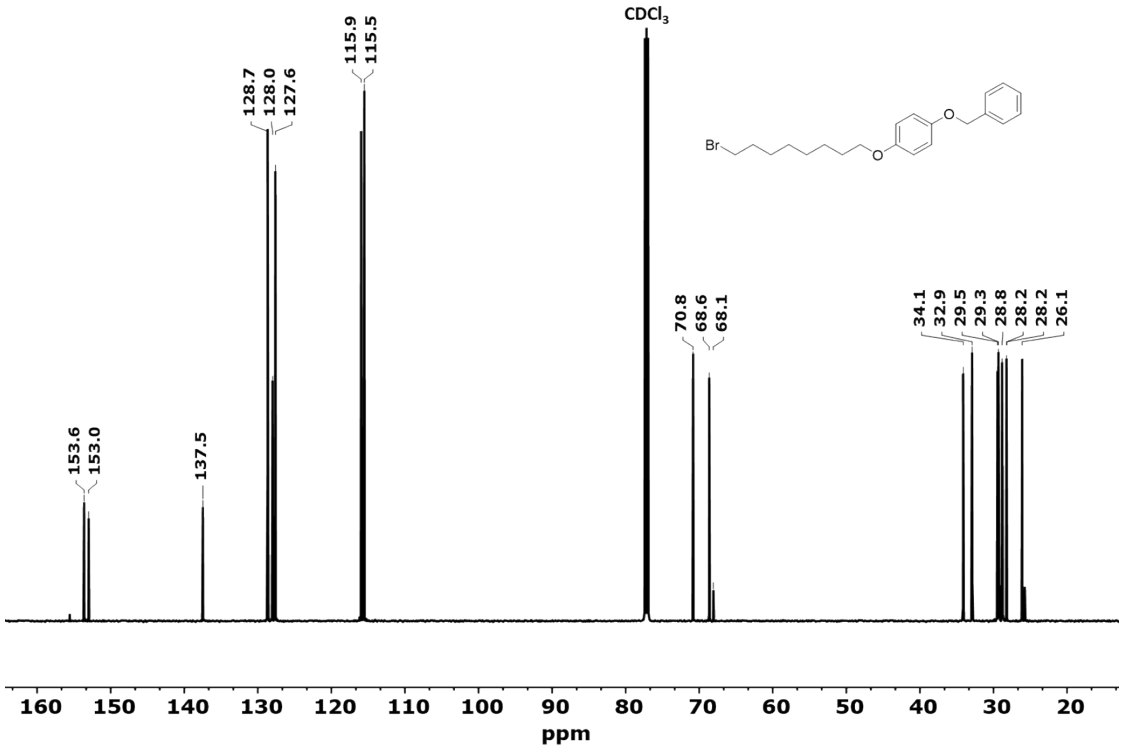

Figure S11. ^{13}CNMR (150 MHz, $CDCl_3$) spectrum of 1-(benzyloxy)-4-(8-bromooctyloxy)benzene.

NMR spectra of difunctionalized pillar[5]arenes:

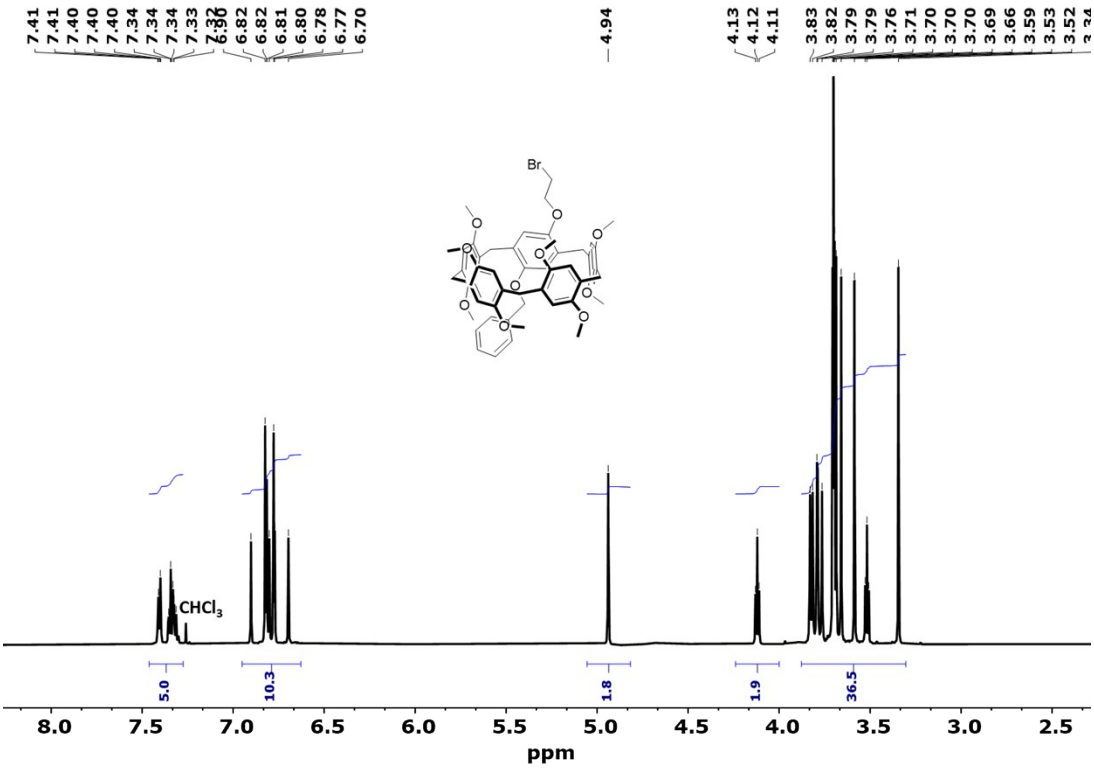

Figure S12. ^{1}HNMR (600 MHz, $CDCl_3$) spectrum of **Pillar-1a.**

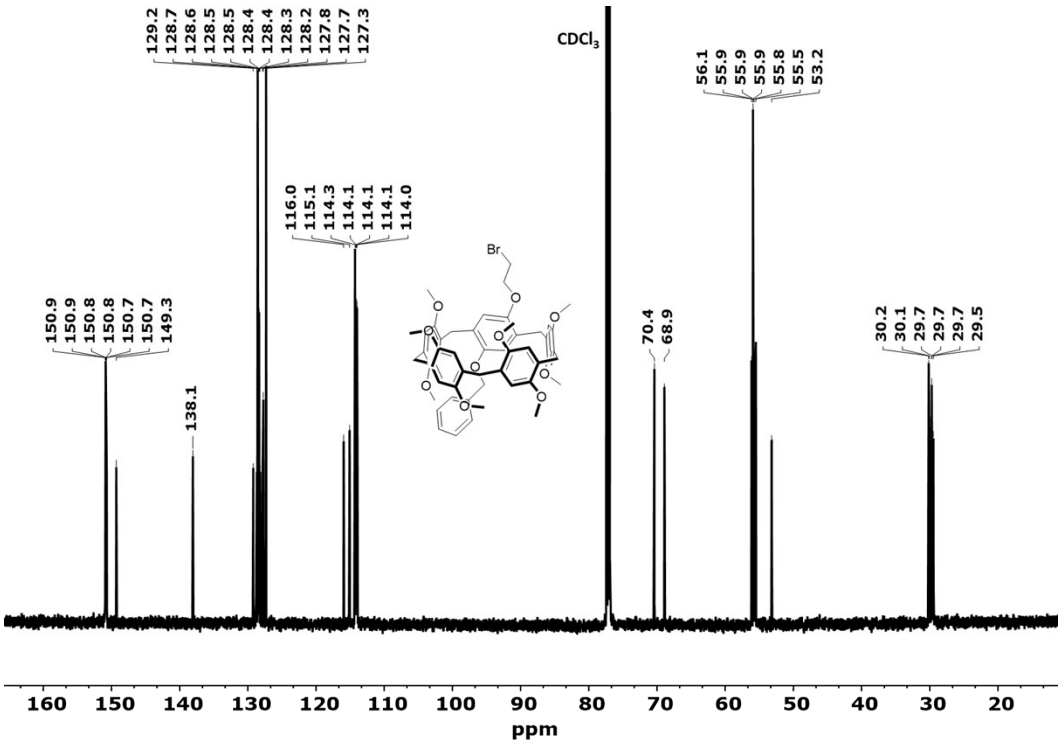

Figure S13. ^{13}CNMR (150 MHz, $CDCl_3$) spectrum of **Pillar-1a**.

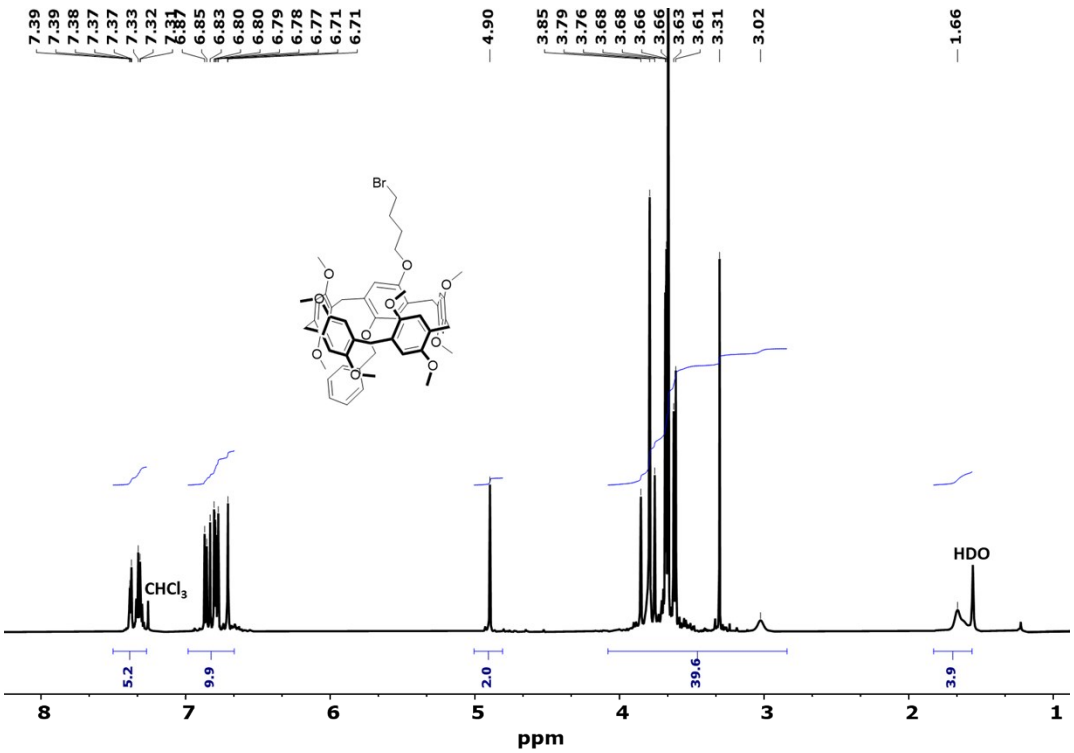

Figure S14. ^{1}HNMR (600 MHz, $CDCl_3$) spectrum of **Pillar-1b**.

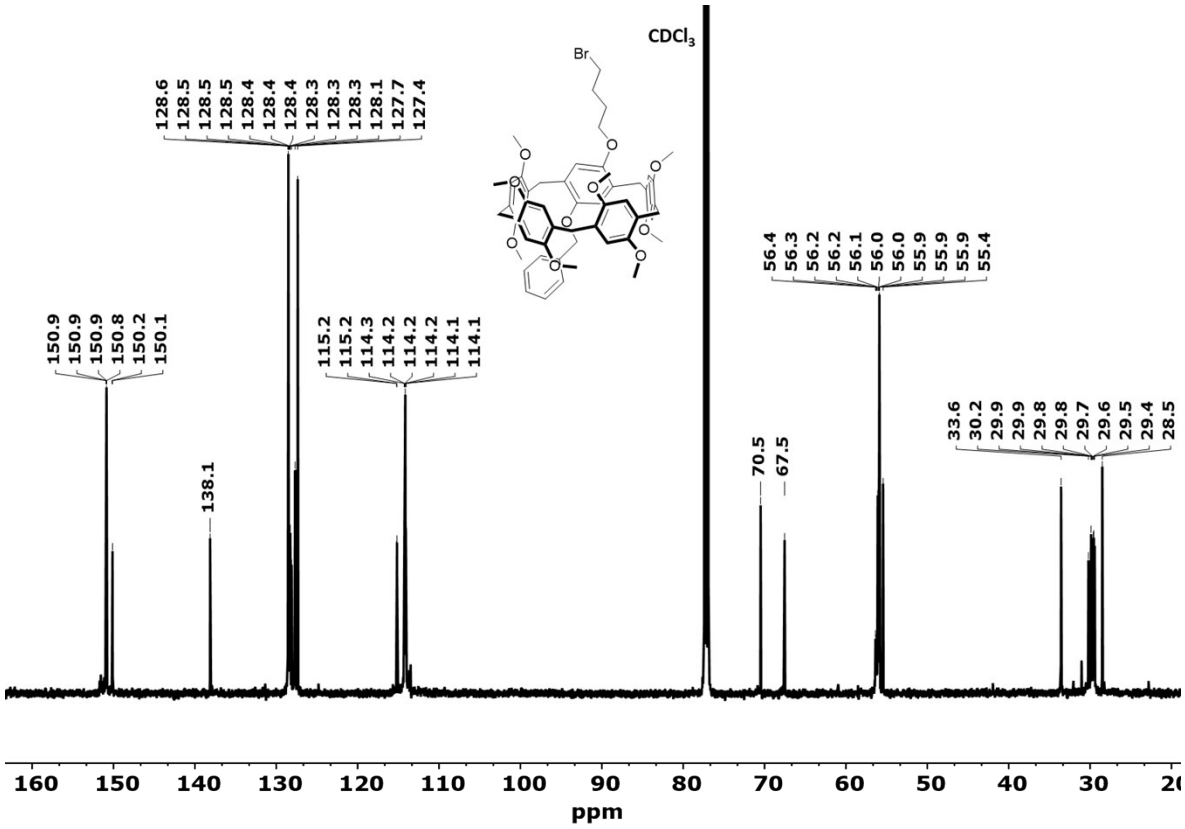

Figure S15. ^{13}CNMR (150 MHz, $CDCl_3$) spectrum of **Pillar-1b**.

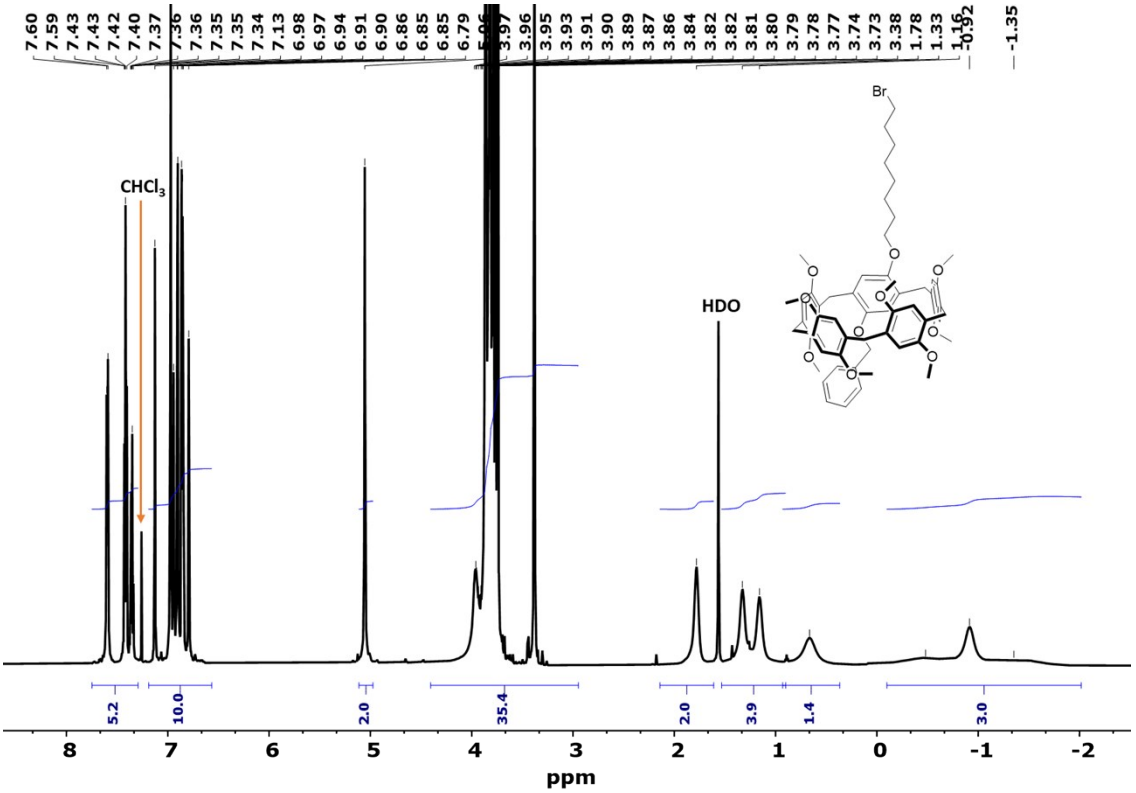

Figure S16. ^{1}HNMR (600 MHz, $CDCl_3$) spectrum of **Pillar-1c**.

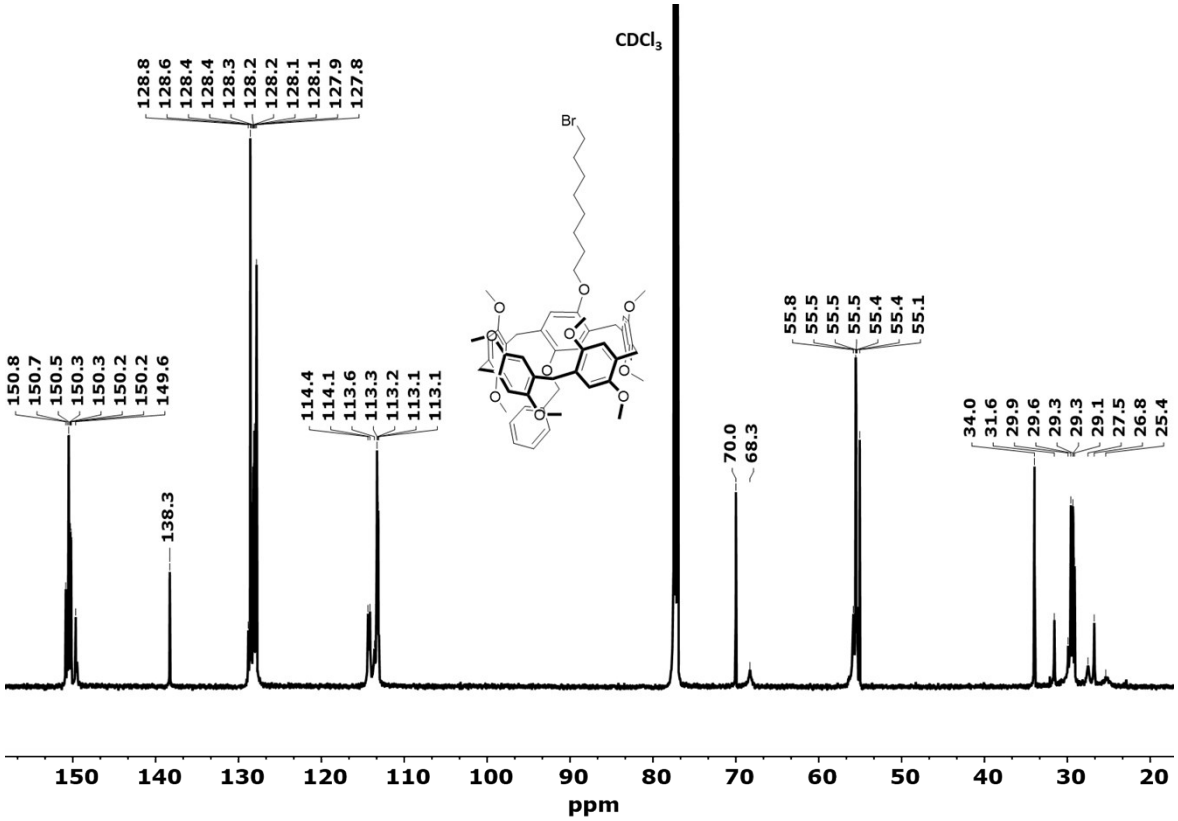

Figure S17. ^{13}CNMR (150 MHz, $CDCl_3$) spectrum of **Pillar-1c**.

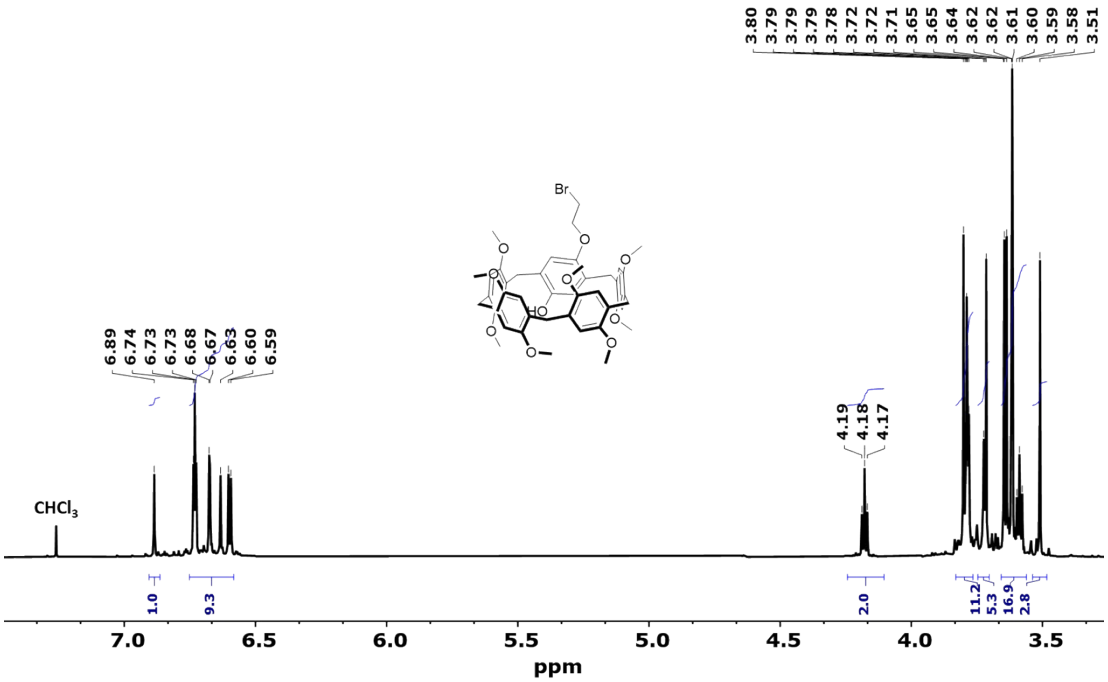

Figure S18. ^{1}HNMR (600 MHz, $CDCl_3$) spectrum of **Pillar-2a**.

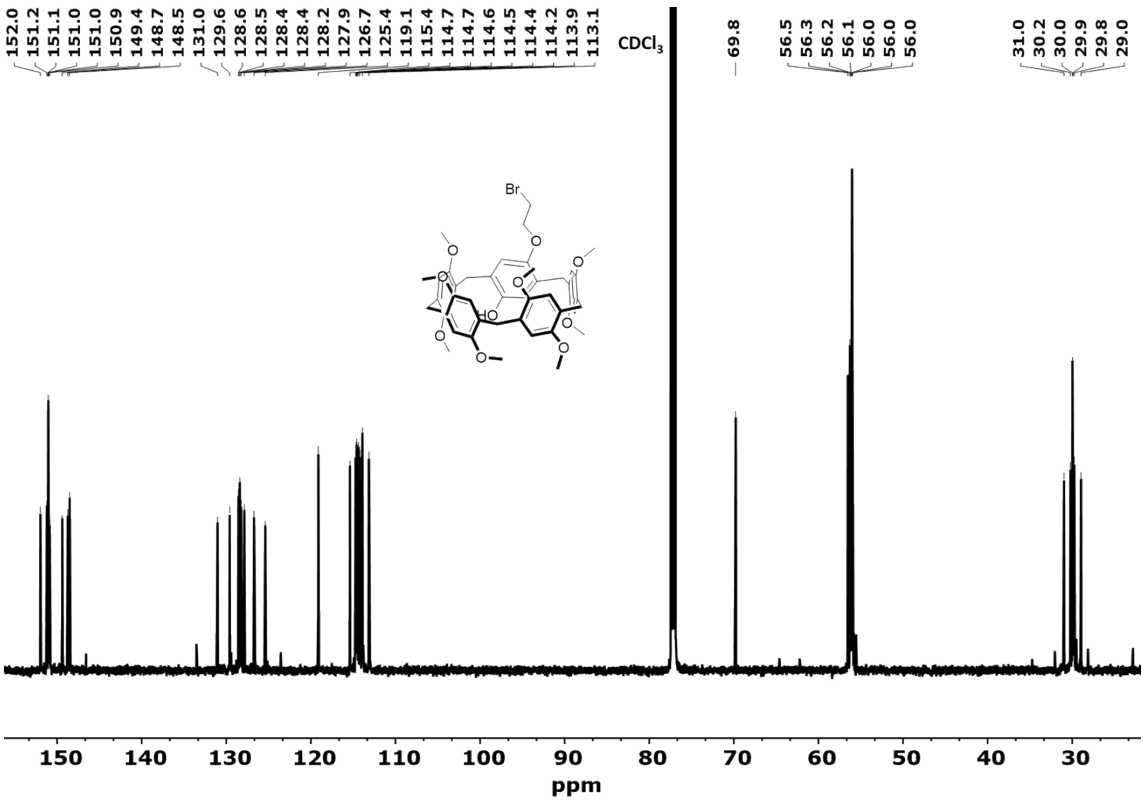

Figure S19. ^{13}CNMR (150 MHz, $CDCl_3$) spectrum of **Pillar-2a**.

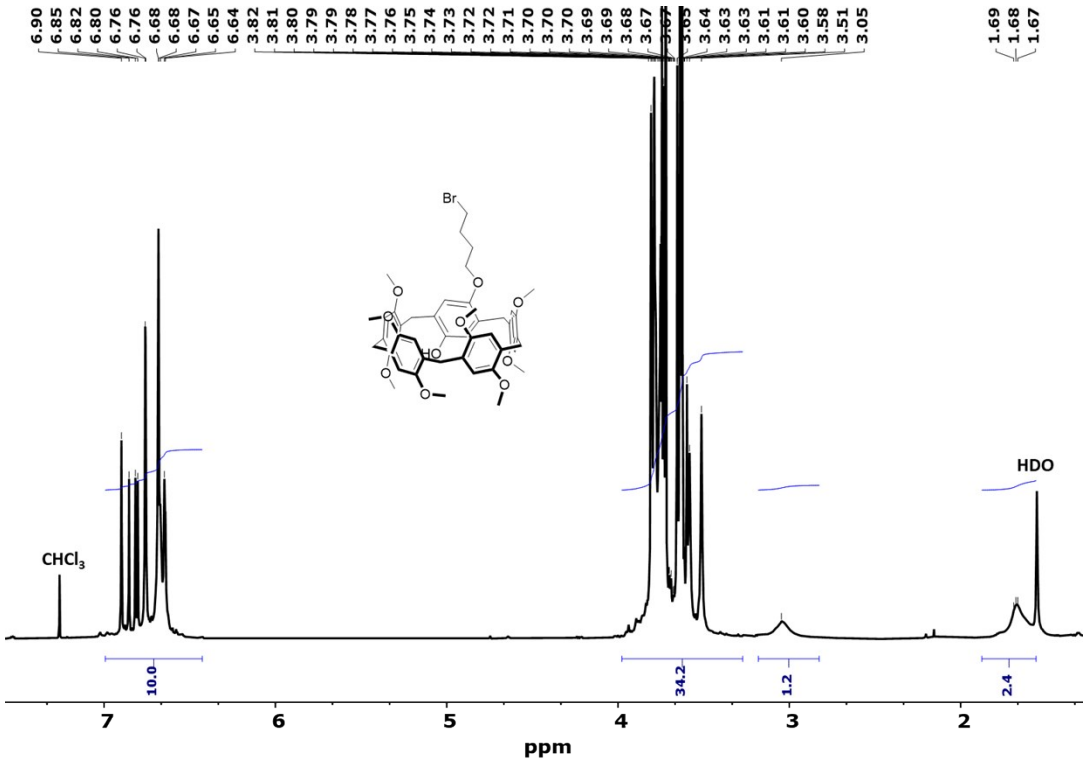

Figure S20. ^{1}HNMR (600 MHz, $CDCl_3$) spectrum of **Pillar-2b**.

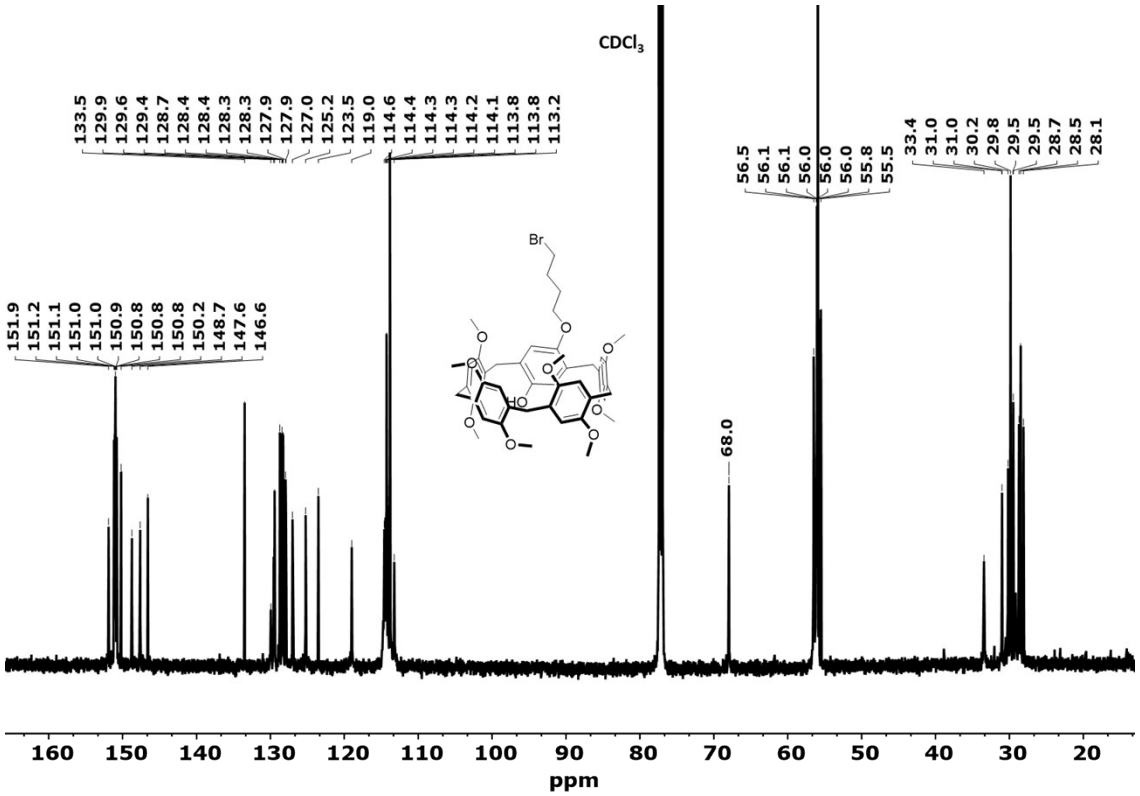

Figure S21. ^{13}CNMR (150 MHz, $CDCl_3$) spectrum of **Pillar-2b**.

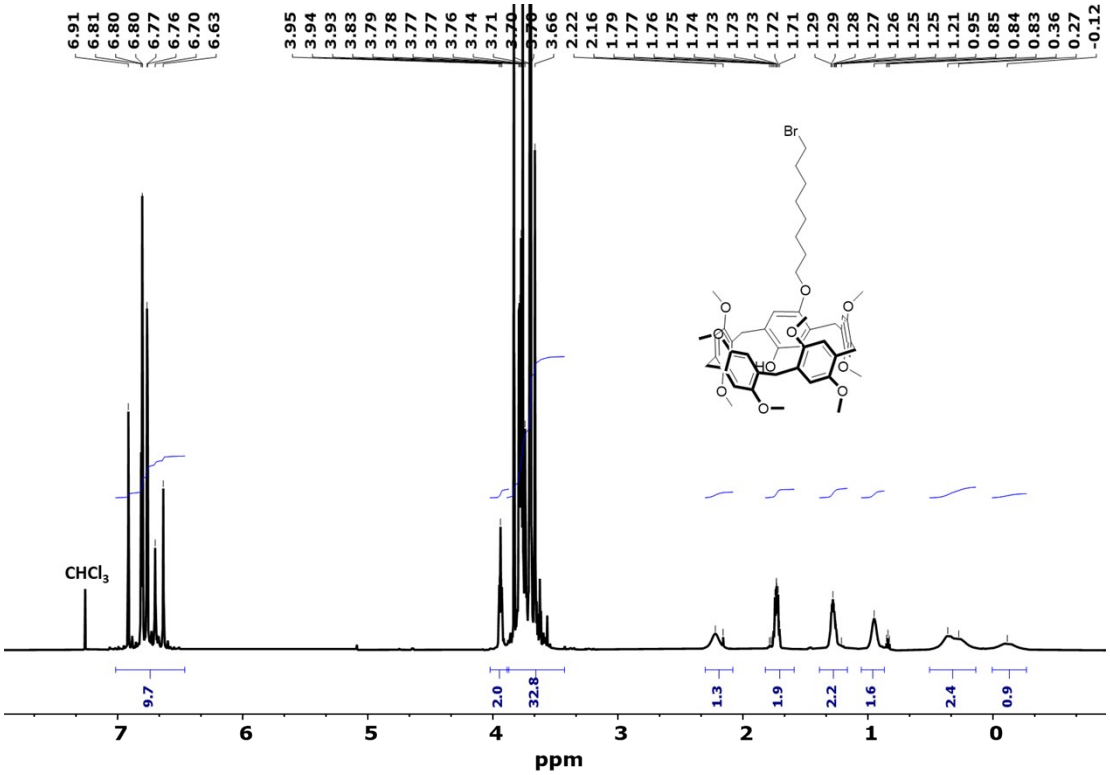

Figure S22. ^{1}HNMR (600 MHz, $CDCl_3$) spectrum of **Pillar-2c**.

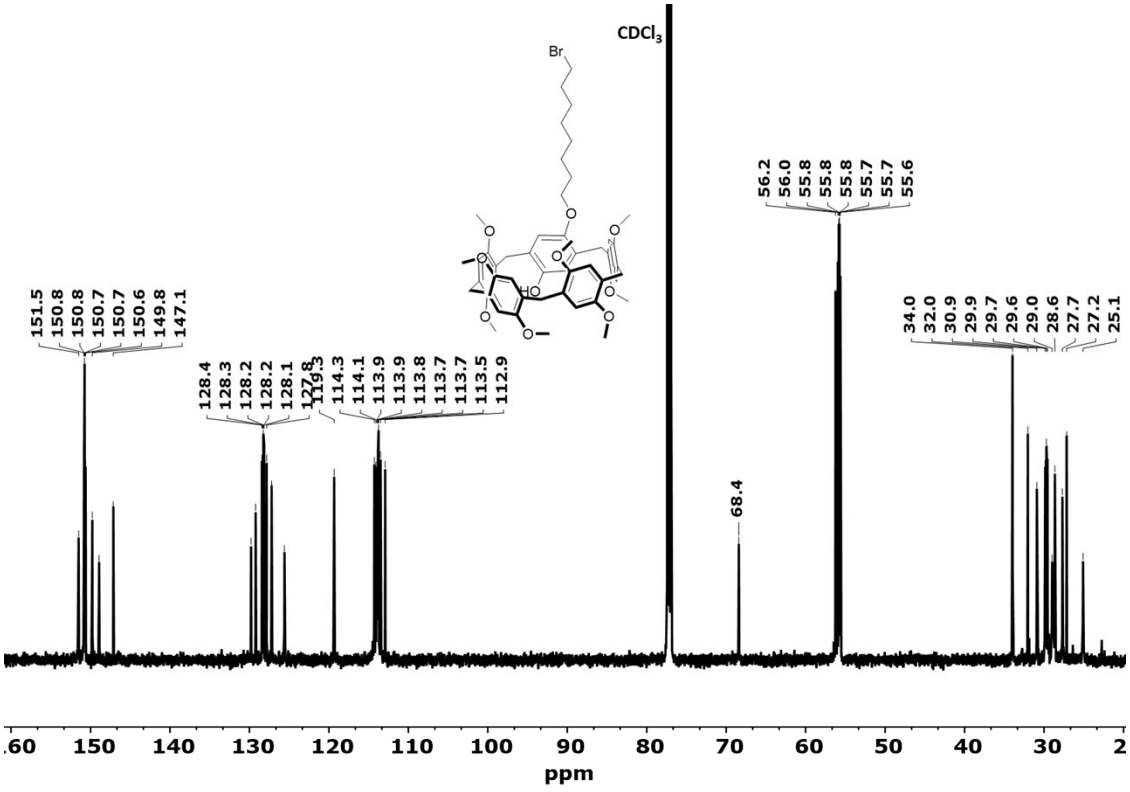

Figure S23. ^{13}CNMR (150 MHz, $CDCl_3$) spectrum of **Pillar-2c**.

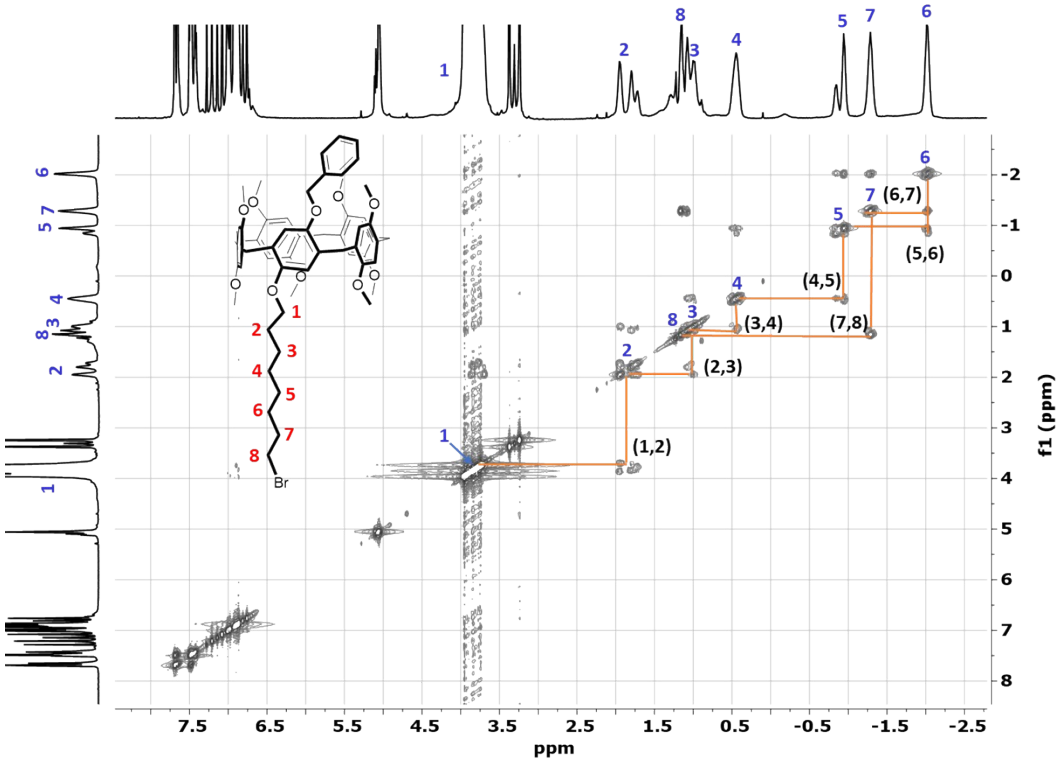

Figure S24. Expanded ^{1}H-^{1}H NMR spectrum (600 MHz, $CDCl_3$ at 233 K) of **Pillar-1c**.

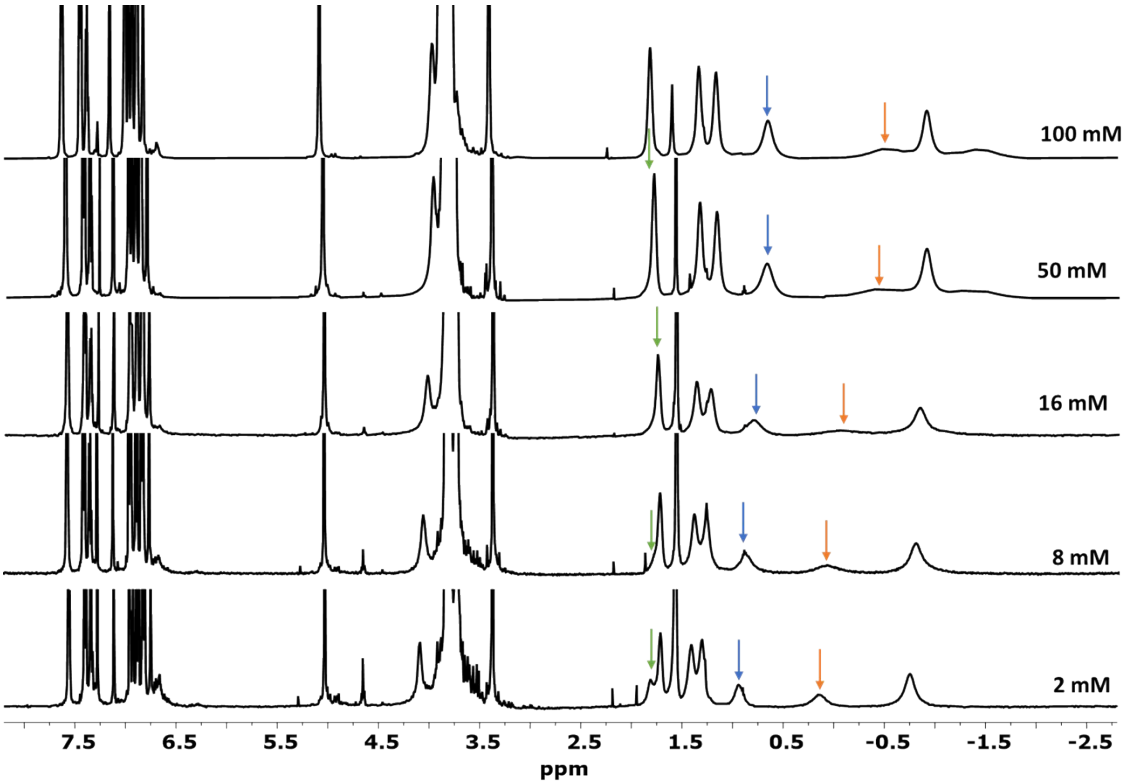

Figure S25. ^{1}H NMR spectra (600 MHz, $CDCl_3$ at 298 K) of **Pillar-1c** at various concentrations.

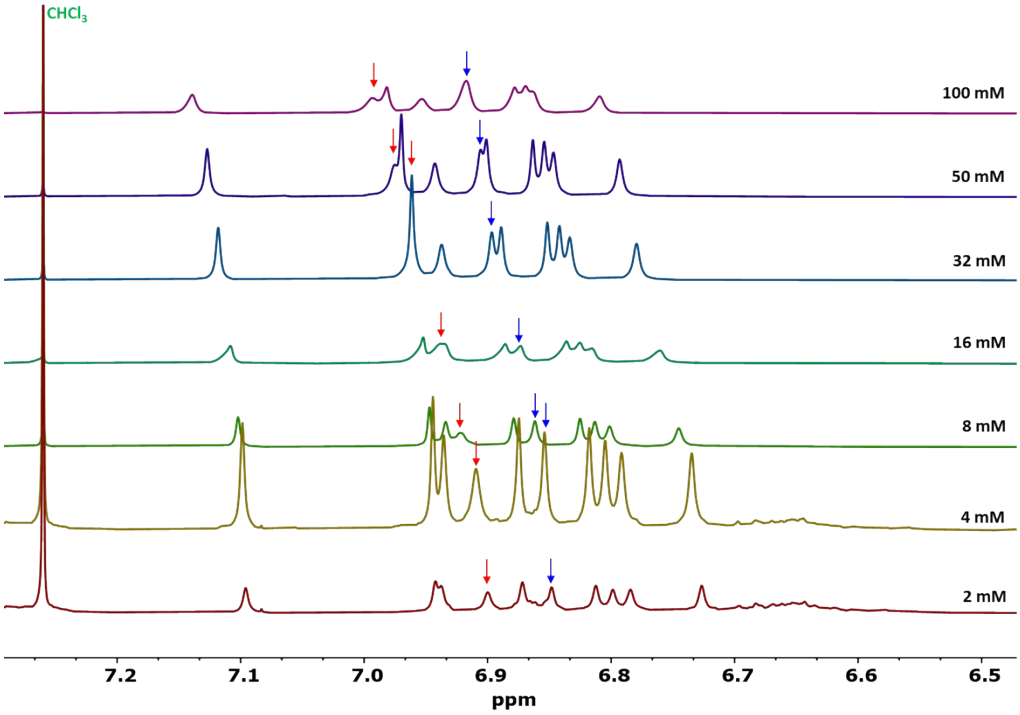

Figure S26. Expanded ^{1}H NMR spectra (600 MHz, $CDCl_3$ at 298 K) for **Pillar-1c** aromatic region at various concentrations.

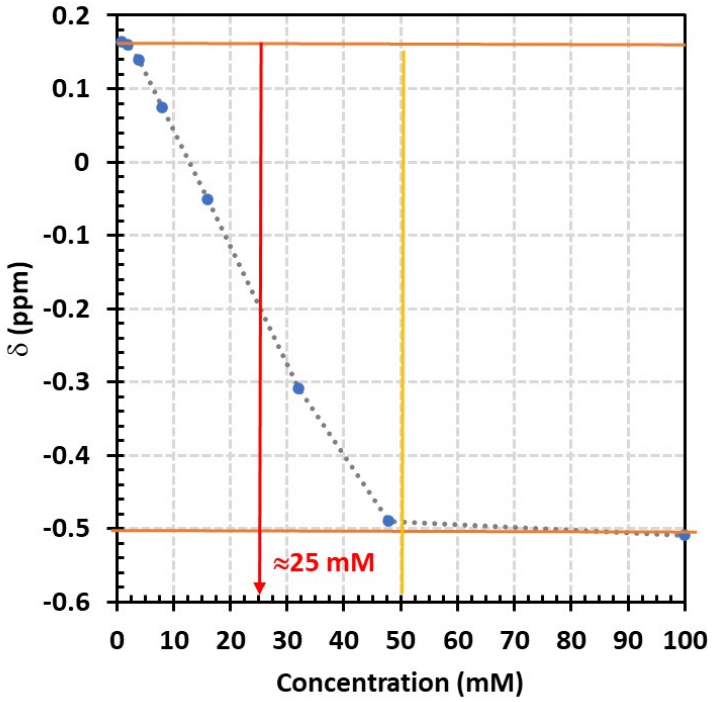

Figure S27. Plot of chemical shif changes (δ) of the methylene proton at 0.22 ppm as a function concentration (600 MHz, $CDCl_3$ at 298 K) for **Pillar-1c**.

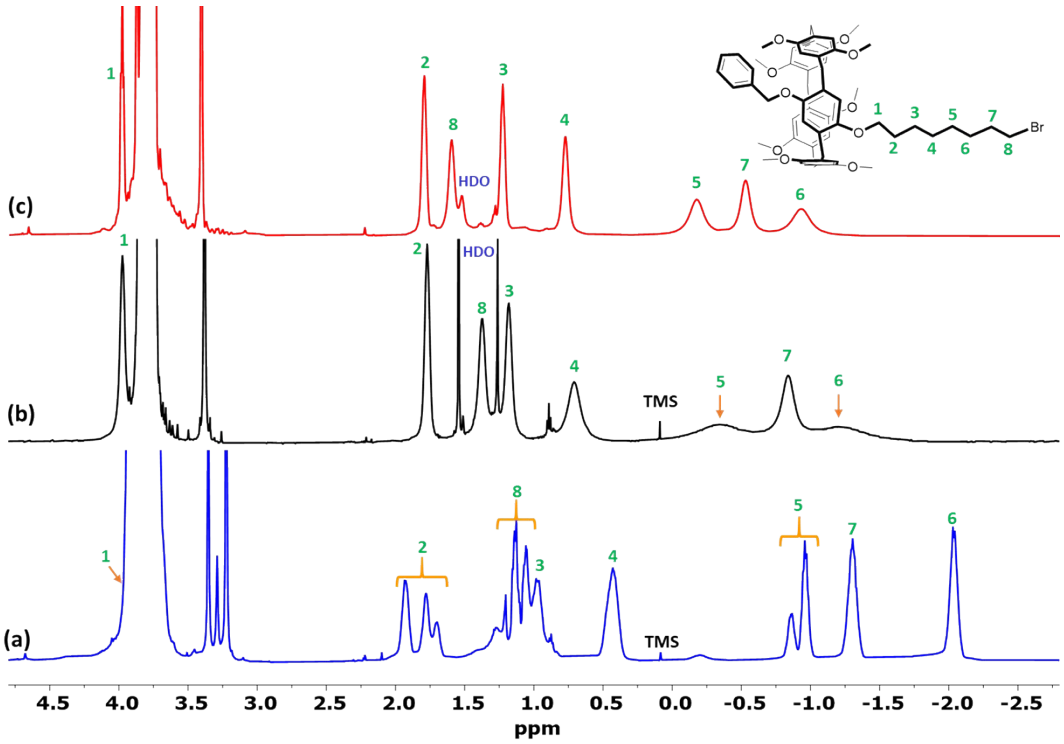

Figure S28. Partial ^{1}H NMR spectra (600 MHz, $CDCl_3$) of **Pillar-1c** at 258 K a), 298 K b) and 318 K b).

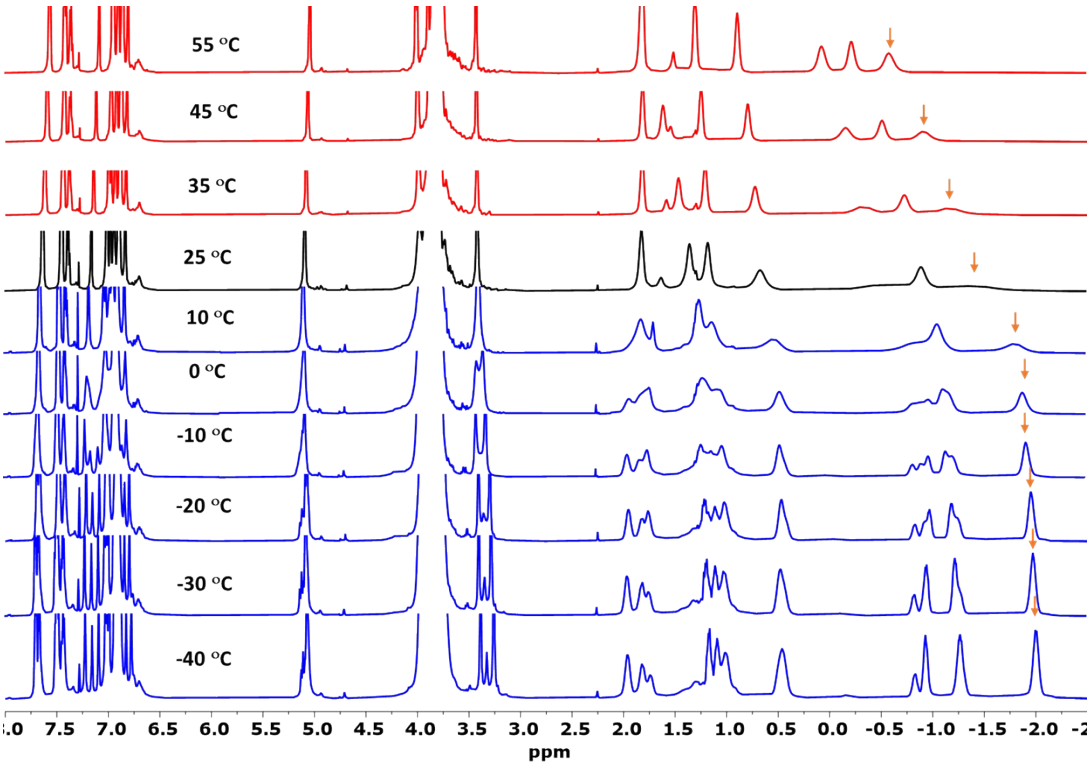

Figure S29. Variable-temperature ^{1}H NMR spectra (600 MHz, $CDCl_3$) of **Pillar-1**

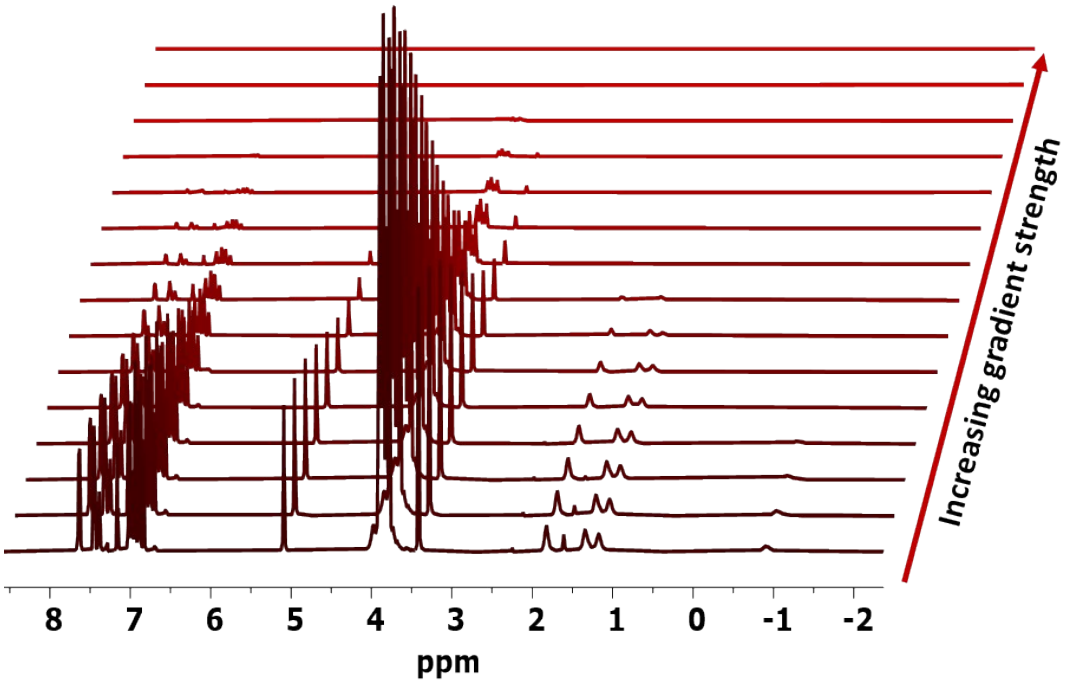

Figure S30. Typical experimental 1D ^{1}H Diffusion traces (600 MHz, $CDCl_3$ at 298 K) a progressive intensity decay as a function of gradient strength for **Pillar-1c**.

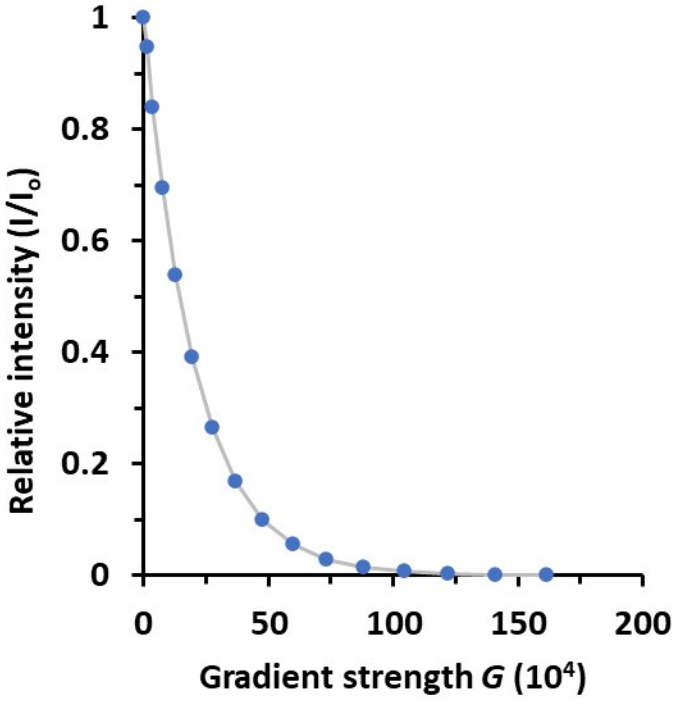

Figure S31. Typical plot of relative intensity (I/I_o) changes of the aromatic protons' region as function of gradient strength *G* (10^4) for **Pillar-1c** in $CDCl_3$ at 298 K.